

# One-dimensional theory of harmonically seeded free-electron laser

Ganesh Tiwari *Brookhaven National Laboratory, Upton, New York 11973, USA*

(Received 10 January 2023; accepted 31 May 2023; published 20 June 2023)

We revisit free-electron laser (FEL) equations in the presence of a planar undulator to investigate effects on longitudinal FEL dynamics upon seeding by a harmonic. For this study, we adopt slowly varying phase approximation, collective variables, and Klimontovich description of particle beams to explore the effects of harmonic seeding on low-gain saturation, low-gain amplification, and exponential growth for on-axis radiation emission. We also investigate the effects of frequency detuning and nonzero energy spread on power gain and growth rate for low-gain and high-gain FELs, respectively.

DOI: [10.1103/PhysRevAccelBeams.26.060701](https://doi.org/10.1103/PhysRevAccelBeams.26.060701)

## I. INTRODUCTION

Madey proposed passing “free” electrons through a periodic magnetic field to extend laser wavelength to x-ray region [1]. Although one could expect to generate coherent radiation of arbitrary wavelength using Madey’s free-electron laser (FEL) idea, practical implementations are often limited by available technologies for particle acceleration and beam manipulation, magnet design and fabrication, and optics for radiation beam transport. In fact, soft and hard x-ray FEL facilities began construction and operation only after 2000s [2–9]. These facilities exploit high-gain configurations such as the self-amplified spontaneous emission (SASE) technique as well as harmonic generation via seeding and/or electron beam manipulation (see Refs. [2–9]). On the other hand, prospects of, and later demonstrations, of Bragg crystals [10] and compound refractive lenses [11] for transporting coherent and intense hard x-ray pulses have sparked significant interest in the cavity based x-ray FELs for both low-gain and high-gain cases [12–20]. In principle, cavity based FELs (CBFELs) allow harmonic lasing of harmonic content ( $h > 1$ ) by filtering the undesired part of the radiation spectrum in optics, thereby extending the possibility of generating coherent, stable, and narrow bandwidth radiation pulses from FEL based light source [21,22]. CBFELs can also be used to seed harmonic content to a FEL via out-coupling schemes [22,23]. Since the field amplitude of this harmonic content becomes higher than that of the spontaneous emission as required by lasing criterion, FEL dynamics evolves primarily under the influence of the harmonic seed.

The follow-up question is straightforward: How do we determine the effects of harmonic seed in the FEL dynamics? While a lot of work has been done on FEL theory since Madey’s FEL idea, here we skim through only relevant work and refer the audience to Refs. [22,24] and within to satisfy their curiosities. Colson derived the FEL pendulum equations by solving for longitudinal electron motion in the presence of radiation and undulator fields [25]; he extended this treatment to apply for the generation of harmonics [26]. While Bonifacio *et al.* [27] applied collective variables approach for high-gain FELs, Kim applied Colson’s formulation along with the microscopic description of electron beams by Klimontovich distribution function to formulate 1D and 3D models for SASE in high-gain FELs [28,29] and brightness functions based gain formula for low-gain FELs [30]. Later, Bonifacio *et al.* studied nonlinear harmonic generation in high-gain FELs with fundamental seed using one-dimensional model [31]; Huang and Kim [32] applied coupled Maxwell-Klimontovich equations to extend this model in three dimension, whereas Freund *et al.* [33] applied a three-dimensional code capable of treating multiple frequencies to study nonlinear harmonic generation. Alternate schemes of variable delay or phase shifting have been proposed to suppress fundamental emission in favor of harmonic generation [34,35]. Yu proposed using a modulator and a radiator configuration with a dispersive element in between to introduce harmonic bunching in the electron beam to improve coherence in harmonic emission [36,37]; Penn *et al.* investigated this scheme for low-gain FELs in Ref. [38]. An extension of Yu’s modulator scheme involves using two modulators instead of one to exploit the echo effect enabling density modulations at a higher harmonic number as proposed by Stupakov and Xiang [39,40]. Feng and colleagues proposed the phase-merging technique based on enhanced harmonic generation to boost FEL efficiency further [41,42]. Moreover, standard FEL codes like TDA3D [43,44], GINGER [45], GENESIS [46],

---

*Published by the American Physical Society under the terms of the Creative Commons Attribution 4.0 International license. Further distribution of this work must maintain attribution to the author(s) and the published article’s title, journal citation, and DOI.*

FAST [47], PUFFIN [48], and MINERVA [49] have been brought into existence and used to compare and evaluate the performance of FEL facilities and mentioned schemes. Recently, Yu extended the low-gain formula with no focusing approximation to achieve harmonic lasing in transverse gradient undulator based FEL [18,50].

Nevertheless, the mentioned theory works are not fully equipped to solve harmonically seeded FEL systems. While one could potentially simulate a harmonically seeded FEL system using standard FEL codes, such studies will be assigned to a limited parameter space and be restricted from generalization. To address the effects of harmonic seed in FEL dynamics, we adopt a slowly changing pondermotive phase description [25,26] and collective variables [27] as well as Klimontovich description of particle beams [29,30]. In this report, we derive equations governing longitudinal dynamics for a FEL in the presence of harmonic seeding and a planar undulator neglecting space charge and recoil effects for on-axis radiation emission. We note that calculation techniques explored here have been previously applied and most expressions thoroughly derived and investigated previously for fundamental radiation seeding [22,24,51]. We tried our best to minimize repetitions of derivations and keep only the pertinent ones necessary for our study here. In addition, we assume that both the seed and emitted radiation are on-axis and odd harmonics of fundamental radiation to comply with 1D model approximation.

The rest of this article is organized as follows: Section II applies single particle motion from Appendix A and slowly changing approximation to obtain pendulum equations governing longitudinal dynamics for single electrons. In Sec. III, we apply the collective variables approach to solve for power gain length using the phase and energy expressions obtained from Sec. II and the Maxwell equation for emitted harmonic radiation from Appendix B. Then, we introduce Klimontovich distribution function for the electron beam to formulate coupled equations governing longitudinal FEL dynamics in Sec. IV; we solve these equations to obtain expressions for the spectral power density of spontaneous radiation, power gain for low-gain amplification, and growth rate in Secs. IV A–IV C, respectively. We wrap up this report in Sec. V.

## II. FEL PENDULUM EQUATIONS

We proceed to derive the FEL pendulum equations for electrons. The electron is under the influence of both undulator and radiation fields with the undulator field as a primary source of particle motion as covered in Appendix A. The energy exchange only occurs between electron and radiation fields. Electrons lose energy via radiation emission and gain energy from seed radiation. Assuming the radiation spectrum consists of all harmonics, we can model the radiation fields as a collection of discrete electromagnetic waves given by

$$\mathbf{E}(z; t) = \hat{x} \sum_h E_0^h \cos(k_h z - \omega_h t + \phi_h), \quad (1)$$

where the waves are polarized in the  $x$  direction and copropagating with the electron beam.  $E_0^h$  is the field amplitude and  $\phi_h$  is the phase of a harmonic  $h$  with wave number  $k_h$  and frequency  $\omega_h$ . The rate of energy transfer from the radiation spectrum of Eq. (1) to an electron is given by the incremental work  $W = \mathbf{F} \cdot \mathbf{v} = -e\mathbf{E} \cdot \mathbf{v}$  where  $e$  is electron charge and  $\mathbf{v}$  is its velocity. Substituting the electron velocity from Eq. (A3a) and field amplitude from Eq. (1), we obtain

$$\begin{aligned} W &= -e\mathbf{E} \cdot \mathbf{v} \\ &= \frac{eKc}{\gamma} \cos(k_u z) \sum_h E_0^h \cos(k_h z - \omega_h t + \phi_h), \end{aligned} \quad (2)$$

with  $\gamma$  being electron's relativistic Lorentz factor and  $K = 0.9343\lambda_u[\text{cm}]B_0[\text{T}]$  is the undulator deflection parameter. Since the rate of energy change for an electron is  $d(\gamma mc^2)/dt$ , we obtain

$$\begin{aligned} \frac{d\gamma}{dt} &= \frac{eK}{\gamma mc} \sum_h E_0^h \cos(k_u z) \cos(k_h z - \omega_h t + \phi_h) \\ &= \frac{eK}{2\gamma mc} \sum_h E_0^h \{ \cos[(k_u + k_h)z - \omega_h t + \phi_h] \\ &\quad + \cos[(k_u - k_h)z + \omega_h t - \phi_h] \}. \end{aligned} \quad (3)$$

The argument in the first cosine term (in second line) gives rise to the particle's slowly varying pondermotive phase in the presence of combined radiation and undulator fields, whereas the second cosine term (in the final line) gives rise to fast oscillations that tend to average to zero. Each harmonic  $h$  has a slowly varying pondermotive phase ( $\theta^h$ ) associated with it (the superscript added to indicate association with harmonic  $h$ ) and the overall pondermotive phase of an electron is the result of contribution from all harmonics, i. e.,  $\theta = \sum_h \theta^h$ . Since the particle arrival time  $t$  is fast varying component as defined in (A4), we assign the average particle time  $\bar{t}$  to define a slowly varying phase  $\psi^h$  given by

$$\psi^h = (k_h + k_u)z - \omega_h \bar{t}. \quad (4)$$

Then, we differentiate on both sides with respect to  $\bar{t}$  to get

$$\frac{d}{d\bar{t}} \psi^h = \frac{d\psi^h}{dz} \bar{v}_z = (k_h + k_u)\bar{v}_z - \omega_h;$$

for  $\omega_h = ck_h$  and  $\bar{v}_z = c[1 - \frac{1+K^2/2}{2\gamma^2}]$ , we rearrange and expand for  $\gamma \gg 1$  to get

$$\begin{aligned} \frac{d\psi^h}{dz} &= k_u + k_h - \frac{ck_h}{\bar{v}_z} \\ &= k_u + k_h - k_h \left[ 1 + \frac{1 + K^2/2}{2\gamma^2} \right] \\ &= k_u \left[ 1 - \frac{k_h}{k_u} \frac{1 + K^2/2}{2\gamma^2} \right]. \end{aligned} \quad (5)$$

The resonant condition for a harmonic radiation emission in planar undulator is given by

$$\frac{k_h}{k_u} = \frac{2h\gamma_r^2}{1 + K^2/2}, \quad (6)$$

where  $\gamma_r$  is the resonant Lorentz factor associated with the resonant energy. For an electron starting with resonant energy, we assume it loses energy via radiation emission in the harmonic seed. If  $\eta^h = (\gamma - \gamma_r)/\gamma_r \ll 1$  is the energy deviation due to radiation emission in the harmonic  $h$  seed, we can rewrite Eq. (5) as

$$\begin{aligned} \frac{d\psi^h}{dz} &= k_u[1 - h(1 + \eta^h)^{-2}] \\ \frac{d\psi^h}{dz} &\approx k_u(1 - h) + 2hk_u\eta^h \\ \frac{d\theta^h}{dz} &\approx 2hk_u\eta^h. \end{aligned} \quad (7)$$

Here we have introduced the reduced phase notation  $\theta^h = \psi^h + (h - 1)k_u z$  to track slowly changing dependence on the particle's energy offset from the FEL resonance condition. Equation (7) is one of the equations that describes pendulumlike behavior of the longitudinal electron motion in FEL.

Now we derive the second equation relevant to the pendulum behavior. For radiation emission at harmonic  $h$  and using the definition of energy deviation  $\eta = (\gamma - \gamma_r)/\gamma_r$  and the definition of ponderomotive phase and average particle time expression of Eq. (A4) which gives

$$k_h z - \omega_h t = \theta^h - hk_u z - \frac{k_h K^2}{k_u 8\gamma^2} \sin(2k_u z),$$

we can rewrite Eq. (3) by expanding cosine in terms of complex exponential as

$$\frac{d\eta^h}{dt} = \frac{eKE_0^h}{4\gamma_r\gamma mc} (e^{ik_u z} + e^{-ik_u z}) \left( e^{i\theta^h - ihk_u z + i\phi_h} \exp \left[ -i \frac{k_h K^2}{k_u 8\gamma^2} \sin(2k_u z) \right] + \text{c.c.} \right).$$

From Jacobi-Anger identity  $e^{ix \sin \varphi} = \sum_{n=-\infty}^{\infty} J_n(x) e^{in\varphi}$ , we get

$$\begin{aligned} &= \frac{eKE_0^h}{4\gamma_r\gamma mc} e^{i(\theta^h + \phi_h)} \sum_{n=-\infty}^{\infty} J_n \left( \frac{k_h K^2}{k_u 8\gamma^2} \right) [e^{i(1-h-2n)k_u z} + e^{-i(1+h+2n)k_u z}] + \text{c.c.} \\ &= \frac{eKE_0^h}{4\gamma_r\gamma mc} e^{i(\theta^h + \phi_h)} \left[ J_{-(\frac{h-1}{2})} \left( \frac{k_h K^2}{k_u 8\gamma^2} \right) + J_{-(\frac{h+1}{2})} \left( \frac{k_h K^2}{k_u 8\gamma^2} \right) \right] + \text{c.c.} \\ &= \frac{eKE_0^h [JJ]_h}{2\gamma_r\gamma mc} \cos(\theta^h + \phi_h). \end{aligned} \quad (8)$$

We kept only the terms associated with factors  $n = (1 - h)/2$  and  $n = -(1 + h)/2$  which give rise to slowly changing phase. We apply two more approximations to obtain a simpler expression for Eq. (8). The first approximation is  $v_z = dz/dt \approx c$  and the second approximation that  $\gamma = \gamma_r(1 + \eta) \approx \gamma_r$ . This results in a simplified version of the energy equation given by

$$\begin{aligned} \frac{d\eta^h}{dz} &= \frac{eKE_0^h [JJ]_h}{2\gamma_r^2 mc^2} \cos(\theta^h + \phi_h) \\ &= \frac{\epsilon_h}{2k_u L_u^2} \cos(\theta^h + \phi_h), \end{aligned} \quad (9)$$

where  $\epsilon_h = \frac{eE_0^h K [JJ]_h}{\gamma_r^2 mc^2} k_u L_u^2$  is the dimensionless field strength. This treatment lets us explore effect of harmonic  $h$  emission in the presence of the same harmonic seed, however we will explore the effect of emission at a different harmonic from seed later. Now we can also express the

Bessel function factor of Eq. (8) in a more convenient form by using the resonance condition [Eq. (6)] and Bessel function identity  $J_{-n}(x) = (-1)^n J_n(x)$  as

$$\begin{aligned} [JJ]_h &= J_{-(\frac{h-1}{2})}(\xi) + J_{-(\frac{h+1}{2})}(\xi) \\ &= (-1)^{(h-1)/2} \left[ J_{(\frac{h-1}{2})}(\xi) - J_{(\frac{h+1}{2})}(\xi) \right], \end{aligned} \quad (10)$$

where  $\xi = hK^2/(4 + 2K^2)$ . For odd harmonics, it is easy to note that alternate  $h$  results in sign flip of  $[JJ]_h$  as  $(-1)^{\frac{h-1}{2}}$  does. Figure 1 clearly shows this pattern for harmonic 3 to 23 with undulator deflection parameter ( $K$ ) ranging from 0 to 5. In other words,  $h = 1, 5, 9, 11, \dots$  take positive values, whereas alternate  $h = 3, 7, 11, 13, \dots$  retain negative values as shown in Fig. 1. Moreover, the absolute value of  $[JJ]_h$  decreases with increasing harmonic number  $h$ . For each harmonic  $h$ , the absolute of  $[JJ]_h$  retains values close to zero and increases slowly toward a fixed value at a threshold  $K$  beyond which it maintains that value as clearly observed for  $h = 3$  in Fig. 1.

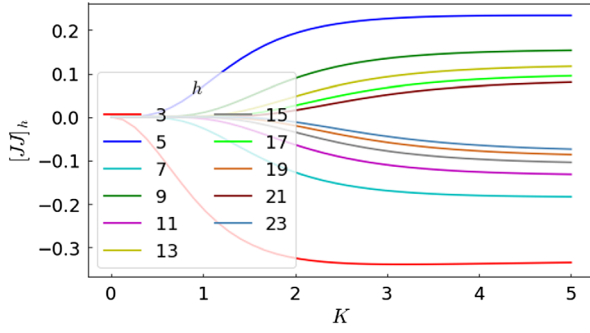


FIG. 1. Plot of Bessel function factor  $[JJ]_h$  for harmonic from 3 to 23 versus undulator deflection parameter  $K$ .

In the presence of a constant electric field of a harmonic  $h$  (i.e.,  $\epsilon_h = \text{constant}$ ),  $\theta^h$  and  $\eta^h$  become conjugate variables of the constant of motion given by

$$H_h = hk_u(\eta^h)^2 - \frac{\epsilon_h}{2k_u L_u^2} [\sin(\theta^h + \phi_h) - \sin(\phi_h)]. \quad (11)$$

At the separatrices ( $\eta^h = 0$  and  $\theta^h = \pm\pi$ ),  $H_h = \frac{\epsilon_h}{k_u L_u^2} \sin \phi_h$  which means

$$\begin{aligned} \eta^h &= \pm \frac{\sqrt{|\epsilon_h|}}{k_u L_u \sqrt{h}} \sqrt{\text{sign}([JJ]_h) \sin\left(\frac{\theta^h}{2} + \phi_h\right) \cos\left(\frac{\theta^h}{2}\right)} \\ &= \pm \eta_{\text{max}}^h \sqrt{\text{sign}([JJ]_h) \sin\left(\frac{\theta^h}{2} + \phi_h\right) \cos\left(\frac{\theta^h}{2}\right)}, \end{aligned}$$

with  $\eta_{\text{max}}^h = \sqrt{|\epsilon_h|}/(k_u L_u \sqrt{h})$ . The motion outside the separatrices is unbounded and unidirectional, whereas the particle exhibits periodic behavior about the stable orbit inside these separatrices which corresponds to the vibrational motion of the pendulum (see Ref. [22] for more details). The latter region is often referred to as pondermotive bucket in which particles are trapped for a constant field. The maximum height of this bucket is  $\eta_{\text{max}}^h$  and is directly proportional to the square root of the absolute value of the Bessel function factor and inversely proportional to square root of the harmonic number  $h$ . Figure 2(a) shows the separatrices in the longitudinal phase space of the electron in odd harmonic potentials for  $h$  ranging from 1 to 15 where the pondermotive bucket is bounded by the solid lines. The bucket boundary is drawn for  $\phi_h = \frac{\pi}{2}$  for  $h = 1, 5, 9, 13$  and  $\phi_h = -\frac{\pi}{2}$  for  $h = 3, 7, 11, 15$ . The bucket size shrinks with increasing harmonic number, indicating less area for trapping electrons and energy exchange. Figure 2(b) shows the ratio of maximum bucket height for different harmonic with respect to that of the fundamental radiation with  $E_0^h = E_0^1$  for  $K$  ranging from 0 to 5. It is clear that bucket height decreases with increasing harmonic number as seen before in Fig. 2(a). For each harmonic number, the maximum bucket height keeps on increasing until a threshold value for  $K$  is reached,

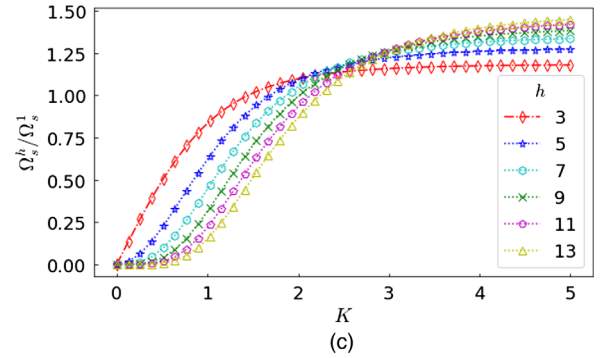
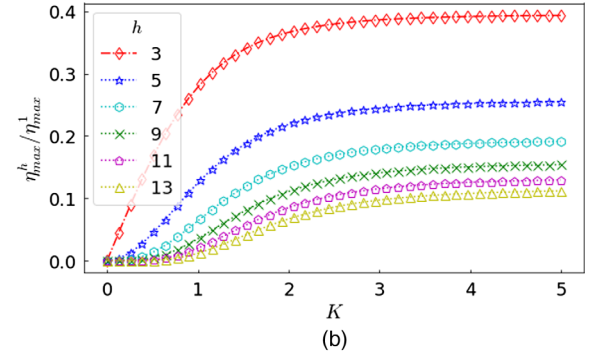
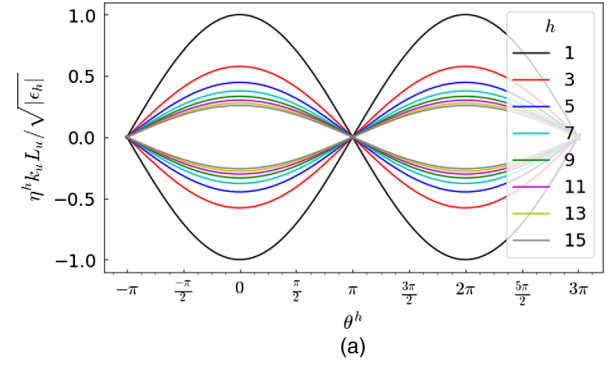


FIG. 2. (a) Separatrices of harmonic potentials in longitudinal phase space for  $\phi_h = \frac{\pi}{2}$  for  $h = 1, 5, 9, 13$  and  $\phi_h = -\frac{\pi}{2}$  for  $h = 3, 7, 11, 15$ . Ratios of (b) maximum bucket height in the presence of harmonic  $h$  with respect to that with fundamental and (c) oscillation frequency near stable points in harmonic  $h$  potential with respect to that in fundamental potential.

beyond which the bucket height remains fixed. For  $h < 10$ ,  $K_{\text{thres}} \approx 3$  as shown in Fig. 2(b).

The oscillatory motion in the pondermotive bucket occurs at a frequency that is dependent on the energy  $H_h$ . However, the motion close to the stable fixed point is similar to that of a simple harmonic oscillator for small phase ( $|\theta^h| \ll 1$ ). In this case, the oscillation wave number is given by

$$\Omega_s = \frac{\sqrt{h|\epsilon_h|}}{L_u}, \quad (12)$$

also known as the synchrotron wave number. The corresponding synchrotron period of the particle in the pondermotive bucket is

$$T_s \equiv \frac{2\pi}{\Omega_s} = \frac{2\pi L_u}{\sqrt{h|\epsilon_h|}}. \quad (13)$$

Figure 2(c) shows the ratio of the synchrotron frequency of a particle in the bucket formed by harmonic  $h$  to that in the bucket formed by the fundamental radiation with the same electric field amplitude. The frequency increases with increasing undulator strength and becomes greater for potentials formed by harmonic  $h > 1$  compared to frequencies of oscillation in a bucket formed by fundamental radiation. There exists a threshold undulator strength after which the frequency of oscillation remains more or less constant for a given harmonic  $h$ . These peculiar behaviors in Fig. 2 may be formulated in terms of scaling laws, however, it is beyond the scope of this article.

Following the discussion in sections 3.3.2 and 7.1.1 of Ref. [22], we can roughly estimate the saturated radiation power in low-gain scenarios in single pass and oscillator based FELs. For a harmonic  $h$ , the maximum saturated power in a single pass FEL would be given by  $P_{\text{sat}}^s \approx P_{\text{beam}}/(\sqrt{h}N_u)$ , where  $N_u$  is the total undulator periods and  $P_{\text{beam}}$  is the power of the electron beam. For cavity based oscillator, the saturated power becomes  $P_{\text{sat}}^{\text{osc}} = P_{\text{sat}}^s/(1-R) \approx P_{\text{beam}}/[(1-R)\sqrt{h}N_u]$ . Here  $R$  is the net power reflectivity of the optical cavity forming the oscillator. It is clear that the saturated power of a harmonic  $h$  gets reduced by the square root of the harmonic number itself when compared to the fundamental. This means that the saturated power of an FEL operating at harmonic  $h$  is lower than that for fundamental radiation, which sets the upper limit on maximum achievable radiation power in an operating low-gain FEL.

### III. COLLECTIVE VARIABLES APPROACH

The FEL pendulum equations (7) and (9) and the Maxwell equation (B6) for emitted radiation in time domain together determine the 1D FEL dynamics. To collect these equations in time domain, we use an alternative expression for energy change equation (9) for the  $j$ th particle after the radiation emission of harmonic  $p$  in the presence of harmonic  $h$  seed given by

$$\frac{d\eta_j^h}{dz} = \chi_p \left( \int d\nu E_\nu(z) e^{i\nu\theta_j^h/h} + \text{c.c.} \right), \quad (14)$$

where  $\chi_p = \frac{eK[JJ]_p}{2mc^2\gamma_r^2}$ . Here we have assumed that  $\nu \approx p$  with  $\nu - p = \Delta\nu$  for  $\Delta\nu \ll 1$  following Appendix B. Hence, we obtain the following set of 1D FEL equations

$$\frac{d\theta_j^h}{dz} = 2hk_u\eta_j^h, \quad (15a)$$

$$\frac{d\eta_j^h}{dz} = \chi_p(E(\theta; z)e^{ip\theta_j^h/h} + \text{c.c.}), \quad (15b)$$

$$\left[ \frac{\partial}{\partial z} + hk_u \frac{\partial}{\partial \theta} \right] E(\theta; z) = -\kappa_p n_e \langle e^{-ip\theta_j^h/h} \rangle_{\Delta_h}. \quad (15c)$$

In the field equation, we have introduced  $\kappa_p = \frac{eK[JJ]_p}{4\epsilon_0\gamma_r}$  and the bunching expression  $\langle e^{-ip\theta_j^h/h} \rangle_{\Delta_h} = (1/N_{\Delta_h}) \sum_{j=1}^{N_e} e^{-ip\theta_j^h/h}$  for  $N_{\Delta_h} = N_{\lambda h}/2\pi = N_{\lambda 1}/2\pi h$ . In other words, only  $N_{\Delta_h}$  electrons with pondermotive phase  $|\theta_j^h - \theta| \leq \Delta\theta/2$  contribute to the coherent radiation emission at position  $z$  [27].

Moreover, we can adopt the dimensionless coordinate system to get insights into FEL evolution (see Refs. [22,24] for instance); we introduce  $\hat{z} = 2k_u\rho z$ ,  $\hat{\eta}^h = \eta^h/\rho$ , and  $a(\theta, \hat{z}) = \frac{\chi_p}{2k_u\rho^2} E(\theta; z)$ . Then, Eq. (15) takes the following form:

$$\frac{d\theta_j^h}{d\hat{z}} = h\hat{\eta}_j^h, \quad (16a)$$

$$\frac{d\hat{\eta}_j^h}{d\hat{z}} = a(\theta; \hat{z})e^{ip\theta_j^h/h} + a(\theta; \hat{z})^* e^{-ip\theta_j^h/h}, \quad (16b)$$

$$\left[ \frac{\partial}{\partial \hat{z}} + \frac{h}{2\rho} \frac{\partial}{\partial \theta} \right] a(\theta; \hat{z}) = -\frac{h\kappa_p\chi_p n_e}{4k_u^2\rho^3} \langle e^{-ip\theta_j^h/h} \rangle_{\Delta_1}. \quad (16c)$$

The coefficient of bunching expression in the right side of field equation becomes unity if we define the Pierce parameter by

$$\rho \equiv \rho_{hp} = \left[ \frac{hn_e\kappa_p\chi_p}{4k_u^2} \right]^{1/3} = \left( \frac{he^2K^2n_e[JJ]_p^2}{32\epsilon_0\gamma_r^3 mc^2 k_u^2} \right)^{1/3}. \quad (17)$$

The Pierce parameter is a real positive number and the subscripts represent emitted harmonic  $p$  and seed harmonic  $h$ . Assuming that  $a(\theta; \hat{z}) \sim 1$  at saturation, we can heuristically claim that the gain length is on the order of  $1/(2k_u\rho_{hp})$  while the saturated power of harmonic  $p$  scales as  $P_p \sim \rho_{hp}P_{\text{beam}}$  in the presence of a harmonic seed  $h$  (refer to Refs. [22,24] for similar analysis with fundamental seed). We note that the bunching expression is normalized to average over electrons present within fundamental wavelength instead of harmonic wavelength for consistency; this choice becomes obvious in Sec. IV C.

To obtain a simpler understanding of the electron beam and radiation interaction in a high-gain FEL, we ignore the radiation slippage (or radiation dependence on  $\theta$ ) in Eq. (16) and introduce the following collective variables:

$$b_h = \frac{1}{h} \langle e^{-ip\theta_j^h/h} \rangle_{\Delta_h} = \langle e^{-ip\theta_j^h/h} \rangle_{\Delta_1}, \quad (18a)$$

$$\mathcal{P}_c = \frac{1}{h} \langle \hat{\eta}^h e^{-ip\theta_j^h/h} \rangle_{\Delta_h} = \langle \hat{\eta}^h e^{-ip\theta_j^h/h} \rangle_{\Delta_1}. \quad (18b)$$

Expression (18a) is bunching factor  $b_h$  associated with density modulation of electron beam upon seeding with harmonic  $h$ . The collective momentum (or energy modulation) in electron beam  $\mathcal{P}_c$  is given by expression (18b). Substituting these variables in Eq. (16) with no slippage approximation and keeping only the lowest order terms in expansion, we obtain the following set of equations:

$$\frac{da}{d\hat{z}} = -b_h, \quad (19a)$$

$$\frac{db_h}{d\hat{z}} = -ip\mathcal{P}_c, \quad (19b)$$

$$\frac{d\mathcal{P}_c}{d\hat{z}} = a. \quad (19c)$$

These linear coupled equations can be rearranged to obtain a third-order differential equation for each collective variable. For the radiation field amplitude  $a$ , it becomes

$$\frac{d^3 a}{d\hat{z}^3} = ipa. \quad (20)$$

$$a(\hat{z}) \approx \frac{1}{3} \left[ a_0 + \frac{\sqrt{3}}{2} \left( \sqrt[3]{p} \mathcal{P}_0 - \frac{b_0}{\sqrt[3]{p}} \right) + \frac{i}{2} \left( \sqrt[3]{p} \mathcal{P}_0 + \frac{b_0}{\sqrt[3]{p}} \right) \right] \exp \left[ \sqrt[3]{p} \frac{\sqrt{3} + i}{2} \hat{z} \right]. \quad (21)$$

Here we substituted initial values  $a(0) = a_0$  for the field amplitude which gets amplified coherently,  $b_h(0) = b_0$  for the bunching, and  $\mathcal{P}_c(0) = \mathcal{P}_0$  for the energy modulation. Nonzero bunching and energy modulation result in radiation power growth in the absence of input radiation  $a(0)$ . The exponential growth power gain length is given by

$$L_{g,hp} = \frac{\lambda_u}{4\pi\sqrt{3}\sqrt[3]{p}\rho_{hp}}, \quad (22)$$

where the Pierce parameter is given by expression (17). Therefore, we have generalized the 1D power gain length formulas for high-gain FEL for harmonic  $p$  emission with harmonic  $h$  seed.

An intuitive idea on the scale of this gain length can be obtained by comparing how harmonic seed and harmonic emission fare against fundamental seeding and/or emission. The gain length ratio for harmonic  $p$  generation with harmonic  $h$  seed compared to fundamental seed becomes

$$\frac{L_{g,hp}}{L_{g,1p}} = \frac{1}{\sqrt[3]{h}}. \quad (23)$$

In other words, seeding with a higher harmonic number  $h$  is more efficient than fundamental seeding for harmonic  $p$  emission by a factor of  $\sqrt[3]{h}$ . Likewise, the gain length ratio

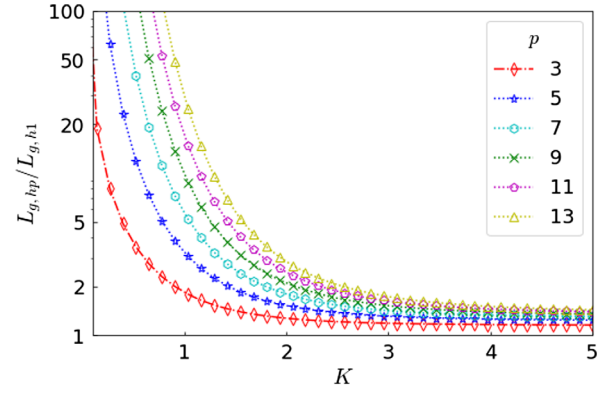


FIG. 3. Plot of gain lengths ratio versus undulator deflection parameter  $K$  for harmonic  $p > 1$  emission with respect to fundamental emission in the presence of harmonic  $h$ .

The complete solution of this equation is derived in Appendix C. The second root results in a growing mode solution. For large propagation distance, the growing mode dominates and drives the laser amplification which can be approximated from Eq. (C4) as

for harmonic  $p > 1$  emission to fundamental emission in harmonic  $h \geq 1$  seed is given by

$$\frac{L_{g,hp}}{L_{g,h1}} = \left( \frac{[JJ]_1}{\sqrt{p}[JJ]_p} \right)^{2/3}. \quad (24)$$

This expression has also been obtained by McNeil *et al.* [34] and Schneidmiller and Yurkov [35] for harmonic emission in a FEL amplifier with fundamental seed. Harmonic  $p > 1$  is favored less than fundamental emission resulting in larger gain lengths for  $p > 1$  as shown in Fig. 3 for  $K$  ranging from 0 to 5. For  $K > 3$ , the gain length for harmonic emission becomes less than twice the gain length for fundamental emission. For larger  $p$  values, the gain length shortens significantly with increasing  $K$  as well, asymptotically approaching  $L_{g,h1}$  for  $K \rightarrow \infty$ . We will cover additional effects of frequency detuning and energy spread on the growth rate for high-gain FELs in Sec. IV C.

#### IV. COUPLED MAXWELL-KLIMONTOVICH EQUATIONS

Various aspects of high-gain FELs such as the SASE process and nonlinear harmonic generation and low-gain FELs can be understood by adopting the microscopic description of electron beam given by Klimontovich

distribution function [28–30,32]; the discrete distribution function for describing these electrons in the longitudinal phase space is

$$F(\theta, \eta; z) = \frac{k_1}{dN_e/dz} \sum_{j=1}^{N_e} \delta[\theta - \theta_j^h(z)] \delta[\eta - \eta_j^h(z)]. \quad (25)$$

Here  $dN_e/dz = I/ec$  is the electron line density for beam current  $I$  and  $N_e$  is the total number of electrons in the beam. Under the assumption that FEL interaction is a perturbative process, the Klimontovich distribution function can be expanded using a coasting beam approximation. Similar techniques of perturbative expansions are also applied in plasma physics (see Refs. [52,53] for instance). In this expansion, the distribution is separated into the smooth background part and a perturbative part, where the perturbative part contains the shot noise and bunchinglike features as follows

$$F(\theta, \eta; z) = \bar{F}(\eta; z) + \delta F(\theta, \eta; z). \quad (26)$$

Here the smooth background function represented by  $\bar{F}(\eta; z)$  is independent of phase and satisfies  $\int d\eta \bar{F}(\eta; z) = 1$ . The continuity equation for the Klimontovich distribution function  $dF(\theta, \eta; z)/dz = 0$  can be broken into two parts as follows:

$$\left[ \frac{\partial}{\partial z} \bar{F} + \frac{d\eta}{dz} \frac{\partial}{\partial z} \delta F \right] + \left[ \frac{\partial}{\partial z} \delta F + \frac{d\theta}{dz} \frac{\partial}{\partial \theta} \delta F + \frac{d\eta}{dz} \frac{\partial}{\partial \eta} \bar{F} \right] = 0. \quad (27)$$

The first bracket in the first line is for the terms that vary slowly along the bunch and also attributes nonlinear harmonic contributions, whereas the second bracket in the second line groups terms with fluctuations from FEL interaction dominated by harmonics. Since these brackets indicate processes that occur at different time scales, each bracket should separately vanish to satisfy continuity condition [22]. Our interest lies in obtaining an equivalent expression for the second bracket in frequency space. In order to do so, we introduce the frequency representation of the distribution function as

$$\begin{aligned} F_\nu(\eta; z) &= \frac{1}{2\pi} \int d\theta e^{-i\nu\theta/h} F(\theta, \eta; z) \\ &= \frac{1}{N_{\lambda 1}} \sum_{j=1}^{N_e} e^{-i\nu\theta_j^h/h} \delta(\eta - \eta_j^h). \end{aligned} \quad (28)$$

This implies  $\delta F(\theta, \eta; z) = \frac{1}{h} \int d\nu e^{i\nu\theta/h} F_\nu(\eta; z)$ . Using the alternative expression for the energy change equation given by Eq. (14), we obtain the Fourier transform version of the second bracket in Eq. (27) to be

$$\left[ \frac{\partial}{\partial z} + 2i\nu k_u \eta \right] F_\nu(\eta; z) = -h\chi_p E_\nu(z) \frac{\partial \bar{F}(\eta; z)}{\partial \eta}. \quad (29)$$

Here we are assuming that the fluctuations are induced by single harmonic  $h$  seed and  $\eta \equiv \eta^h$  for harmonic  $p$  emission in that seed. Using the definition of  $F_\nu$  from Eq. (28) and since  $\nu \approx p$  for  $\Delta\nu \ll 1$  (i.e.,  $\kappa_\nu \equiv \kappa_p$ ), Eq. (B5) for field evolution of harmonic  $p$  when seeded by harmonic  $h$  becomes

$$\left[ \frac{\partial}{\partial z} + i\Delta\nu k_u \right] E_\nu(z) = -\kappa_p n_e \int d\eta F_\nu(\eta; z). \quad (30)$$

The evolution of radiation field and electron beam fluctuations in the FEL can be now solved using Eqs. (29) and (30).

A complete solution of the coupled Maxwell-Klimontovich equations (29) and (30) can be obtained by using Laplace transform [28,54] given by

$$S_{\nu, \mu} = \int_0^\infty dz e^{i2\mu\rho k_u z} S_\nu(z). \quad (31)$$

Here  $S$  is a dummy representation for  $E$  and  $F$ . This allows us to obtain solution for  $S_\nu(z)$  using the inverse Laplace transform given by

$$S_\nu(z) = -\frac{\rho k_u}{\pi} \oint d\mu e^{-i2\mu\rho k_u z} S_{\nu, \mu}. \quad (32)$$

$\rho$  is the FEL scaling parameter introduced in Eq. (17) for dimensionless equations. After careful calculation steps and substituting for  $F_\nu(\eta, 0)$  from Eq. (28), the electric field amplitude becomes

$$E_\nu(z) = \oint \frac{d\mu}{2\pi i} \frac{e^{-i2\mu\rho k_u z}}{D(\mu)} \left[ E_\nu(0) + \frac{i\kappa_p n_e}{2k_u \rho N_{\lambda 1}} \sum_{j=1}^{N_e} \frac{e^{-i\nu\theta_j(0)/h}}{(\frac{\nu\eta_j(0)}{\rho} - \mu)} \right], \quad (33)$$

where the dispersion function  $D(\mu)$  is given by

$$D(\mu) \equiv \mu - \frac{\Delta\nu}{2\rho} - \nu \int d\eta \frac{\bar{F}(\eta)}{(\frac{\nu\eta}{\rho} - \mu)^2}. \quad (34)$$

The radiation evolution in a FEL is mainly dictated by the poles of  $1/D$ , which can be obtained from the roots of  $D(\mu) = 0$ . For  $\rho$  given by Eq. (17) and in the limits of vanishing energy spread, i.e.,  $\bar{F}(\eta) \rightarrow \delta(\eta)$ ,  $D(\mu) = 0$  becomes

$$\begin{aligned} \mu - \frac{\Delta\nu}{2\rho} - \frac{\nu}{\mu^2} &= 0, \\ \mu^2 \left( \mu - \frac{\Delta\nu}{2\rho} \right) &= \nu. \end{aligned} \quad (35)$$

For the FEL resonance condition,  $\Delta\nu = 0$  and  $\mu^3 = p$  which has three solutions  $\mu = \sqrt[3]{p}[1, \frac{i\sqrt{3}-1}{2}, \frac{1-i\sqrt{3}}{2}]$ , as covered in Sec. III and Appendix C, with the second root representing growing solution from Eq. (33). In the exponentially growth regime, the radiation power grows as  $P \propto e^{4\Im(\mu_2)\rho k_u z}$  along the undulator [22,28], where  $\Im(\mu_2) = (p)^{1/3}\sqrt{3}/2$ . The gain length in this exponential growth region is effectively given by Eq. (22). Since we already covered the behavior of gain length for both harmonic seeding and harmonic emission in Sec. III, we carry on to investigate features of spontaneous emission and low-gain and high-gain scenarios. For spontaneous and low-gain radiation emission, we can expand the inverse of the dispersion function in the limits of the vanishing Pierce parameter, i.e.,  $\rho \rightarrow 0$  as follows:

$$\frac{1}{D(\mu)} = \frac{1}{\mu - \Delta\nu/2\rho} + \frac{\nu}{(\mu - \Delta\nu/2\rho)^2} \int d\eta \frac{\bar{F}(\eta)}{(\frac{\nu\eta}{\rho} - \mu)^2}. \quad (36)$$

The first term in the expansion on the right side yields spontaneous radiation whereas low-gain amplification can be studied by keeping the last term in the second line.

### A. Spontaneous radiation

In the absence of input radiation, the FEL process begins with spontaneous emission. From Eqs. (33) and (36), the field amplitude of the spontaneous radiation at any location  $z$  along the undulator is given by

$$E_\nu(z) = \frac{i\kappa_p n_e}{2k_u N_{\lambda 1}} \sum_{j=1}^{N_e} \frac{e^{-i\nu\theta_j/h} e^{-i\Delta\nu k_u z}}{\nu\eta_j - \Delta\nu/2} [1 - e^{-i2(\nu\eta_j - \Delta\nu/2)k_u z}]. \quad (37)$$

Here we applied Cauchy's residue theorem to integrate over  $\mu$  and  $\eta_j = \eta_j(0)$  and  $\theta_j = \theta_j(0)$  represent initial scaled energy shift and phase of the  $j$ th particle, respectively. Assuming that the initial phase distributions are uncorrelated [22,28], we can express the power spectral density of spontaneous radiation at the undulator end as follows:

$$\frac{dP}{d\omega} = \gamma_r^2 m c^2 N_u^2 \left(\frac{\lambda_1^2}{\mathcal{A}_{rr}}\right) \left(\frac{I}{I_A}\right) \left(\frac{K[JJ]_p}{(1+K^2/2)}\right)^2 \times \int d\eta \bar{F}(\eta) \left(\frac{\sin[2\pi N_u(\nu\eta - \Delta\nu/2)]}{2\pi N_u(\nu\eta - \Delta\nu/2)}\right)^2, \quad (38)$$

where  $I_A = 4\pi\epsilon_0 m c^3/e \approx 17045\text{A}$  is the Alfvén current and  $\bar{F}(\eta)$  is the energy distribution of the electron beam. Besides depending on factors in the first line such as beam current ( $I$ ), resonant relativistic Lorentz factor  $\gamma_r$ , and undulator strength  $K$  and length  $N_u = L_u/\lambda_u$ , the spontaneous radiation spectral power density depends on frequency/energy detuning as well as energy distribution of

the electron beam as indicated by the integral in the second line. For comparative analysis of spontaneous power density for electron beams having a uniform or Gaussian energy distribution, we adopt scaled parameters given by

$$x = 2\pi N_u(\nu\eta - \Delta\nu/2) \quad \text{and} \quad y = 2\pi\nu\sigma_\eta N_u.$$

$\sigma_\eta$  is the rms energy spread in a Gaussian distribution. For  $C_p = (\gamma_r^2 m c^2 N_u^2) \left(\frac{\lambda_1^2}{\mathcal{A}_{rr}}\right) \left(\frac{I}{I_A}\right) \left(\frac{K[JJ]_p}{(1+K^2/2)}\right)^2$ , Eq. (38) reduces to

$$\frac{dP}{d\omega} = C_p \int dx \bar{F}(x, y) \left(\frac{\sin x}{x}\right)^2. \quad (39)$$

For an electron bunch with uniform and large energy spread ( $\sigma_\eta \geq 10^{-3}$ ) typical of laser-driven plasma accelerators [55–59], we can effectively approximate  $\bar{F}(x, y) \approx 1/4y$ , where we assumed the uniform distribution to have half-width equivalent to a Gaussian distribution's radius  $2\sigma_\eta (\equiv 2y)$ . In this simple approximation,  $dP/d\omega = C_p \pi/4y$ , where the subscript  $p$  indicates harmonic  $p$ . The increase in energy spread results in a decrease in spontaneous emission; this follows intuitively as a large energy spread brings more electrons out of resonance condition [Eq. (6)] necessary for radiation emission at a desired wavelength.

For practical constraints in energy spread of linear accelerators and storage rings ( $\sigma_\eta \leq 10^{-3}$ ), we evaluate the integral numerically for Gaussian distribution given by

$$\bar{F}(x, y) = \frac{1}{\sqrt{2\pi}y} \exp\left(-\frac{(x-x_0)^2}{2y^2}\right)$$

within the limits of  $[-3y, 3y]$ . Figure 4(a) shows the scaled power density of spontaneous radiation against scaled variables  $x_0 = 2\pi N_u(\nu\eta_0 - \Delta\nu/2)$  and  $y$ . The density is peaked at  $x \approx 0$ , corresponding to  $\eta_0 \approx 0$ , for harmonic  $p$  ( $\Delta\nu = 0$ ) when  $y < 0.5$ . For  $y > 0.5$ , the spectral power density drops significantly while maintaining nonzero values for  $|x| \leq 5$ . A simple comparison of the spontaneous spectral power density of harmonic content to fundamental at a tuned value of  $x_0 \approx 0$  can be made by the following estimate:

$$\frac{dP/d\omega|_p}{dP/d\omega|_1} = \frac{C_p}{C_1} = \left(\frac{[JJ]_p}{[JJ]_1}\right)^2 \quad (40)$$

as shown in Fig. 4(b). For  $K > 2.5$ , the harmonic content power density scales roughly between 0.01 and 0.1 of fundamental radiation. The spontaneous emission of harmonic content is suppressed significantly at  $K < 2$  with higher harmonic suffering further reduction. At  $K \approx 1$ , the third harmonic fares quite well to  $\sim 0.2$ , whereas  $p \geq 9$  attenuates by a factor of  $10^{-4}$  and more. This implies that

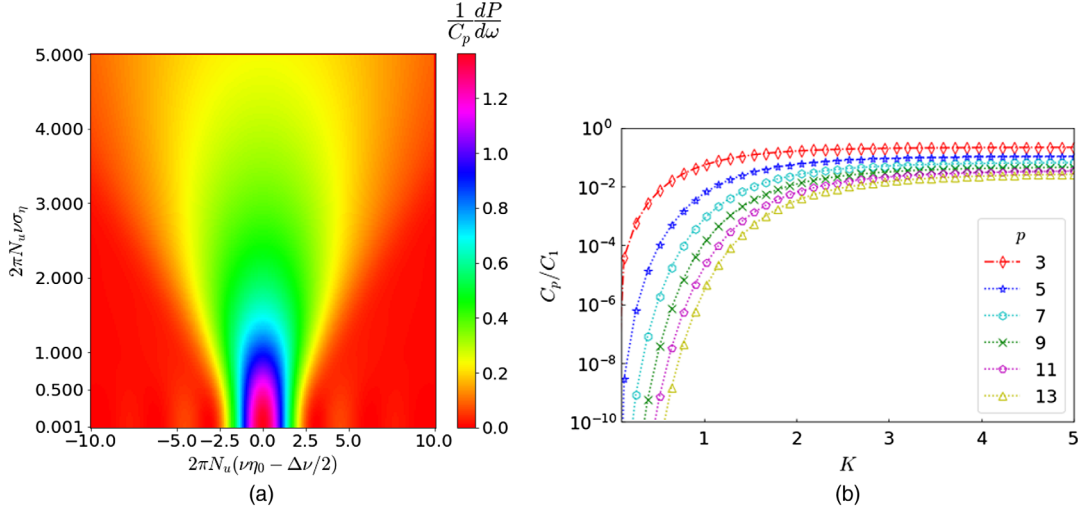


FIG. 4. (a) Density plot of normalized spectral power density  $(1/C_p)dP/d\omega$  versus scaled detuning factor  $x_0 = 2\pi N_u(\nu\eta_0 - \Delta\nu/2)$  and scaled energy spread  $y = 2\pi N_u\nu\sigma_\eta$ . (b) Ratio of spectral power density of spontaneous radiation for harmonic  $p$  to fundamental at tuned  $x_0 \approx 0$ . The  $y$  axis in (b) is in  $\log_{10}$  scale.

using electron beam shot noise does not favor harmonic spontaneous emission at tuned energy for  $K < 2$ .

### B. Low-gain amplification

Although we can use the second term in Eq. (36) to obtain first-order amplification in the low-gain limit, we

revert to a well-known perturbation approach to obtain power gain in the low-gain scenario [30]. In this case, Eqs. (29) and (30) can be solved using iterative perturbation expansion, after which the electric field amplitude of the emitted radiation can be expressed in terms of the electric field at the undulator center as follows:

$$E_\nu(L_u) = \mathcal{G}\left(\frac{L_u}{2}\right)E_\nu\left(\frac{L_u}{2}\right) - \kappa_p n_e \int_0^{L_u} dz \mathcal{G}(L_u - z) \int d\eta e^{-i2\nu k_u \eta z} F_\nu(\eta; 0) \\ + h\chi_p \kappa_p n_e \int_0^{L_u} dz \mathcal{G}(L_u - z) \int d\eta e^{-i2\nu k_u \eta z} \int_0^z ds e^{i2\nu k_u \eta s} E_\nu(s) \frac{\partial \bar{F}(\eta; s)}{\partial \eta},$$

where  $\mathcal{G}(z) = e^{-i\Delta\nu k_u z}$  is the homogenous solution. The first term appears from the input coherent radiation, the second term corresponds to the spontaneous undulator radiation, and the third term is the result of FEL interaction between the electron beam and radiation field. Ideally, we

would solve iteratively to find the evolving radiation field in the undulator. However, an appropriate approximation for  $E_\nu(s) = \mathcal{G}(s - \frac{L_u}{2})E_\nu(\frac{L_u}{2})$  can be used for weak interaction between electron beam and radiation field. In this case, the electric field can be conveniently expressed as

$$E_\nu(L_u) = \mathcal{G}\left(\frac{L_u}{2}\right)E_\nu\left(\frac{L_u}{2}\right) - \kappa_p n_e \mathcal{G}\left(\frac{L_u}{2}\right) \int_0^{L_u} dz \int d\eta U_\nu(\eta; z) F_\nu(\eta; 0) \\ + h\chi_p \kappa_p n_e \mathcal{G}\left(\frac{L_u}{2}\right)E_\nu\left(\frac{L_u}{2}\right) \int d\eta \int_0^{L_u} dz U_\nu(\eta; z) \int_0^z ds U_\nu^*(\eta; s) \frac{\partial \bar{F}(\eta; L_u/2)}{\partial \eta}. \quad (41)$$

Here we introduced 1D undulator field  $U_\nu(\eta; z) = \exp[-i\Delta\nu k_u(\frac{L_u}{2} - z) - i2\nu\eta k_u z]$  and the transformation of  $\bar{F}(\eta; s) \rightarrow \bar{F}(\eta; L_u/2)$  follows naturally with the field transformation. Since the field is complex in nature, the gain of the field amplitude is complex. Therefore, it is more convenient to obtain power gain by computing absolute

square of field amplitude in the above expression. The absolute square of the first term gives input power, whereas the square of the second term gives spontaneous undulator radiation power. The cross terms involving the second term (spontaneous radiation) sum over all particle phases leading to zero. The lowest order power amplification appears from

the cross terms involving the first and third terms [22]. Hence, 1D FEL power gain is given by

$$G = \frac{P_{\text{out}} - P_{\text{in}}}{P_{\text{in}}} = h\chi_p \kappa_p n_e \int d\eta \int_0^{L_u} dz \int_0^{L_u} ds U_\nu^*(\eta; z) U_\nu(\eta; s) \frac{\partial \bar{F}(\eta)}{\partial \eta}.$$

Further simplification comes from substituting  $\bar{z} = z - L_u/2$  and  $\bar{s} = s - L_u/2$ . This changes the limits of  $z$  and  $s$  integrals to  $-L_u/2$  and  $L_u/2$  from 0 and  $L_u$ , respectively. Moreover, the product of the undulator field takes the following form:

$$U_\nu^*(\eta; z) U_\nu(\eta; s) = U_\nu^*(\eta; \bar{z}) U_\nu(\eta; \bar{s}) = \exp[i(2\nu\eta - \Delta\nu)k_u(\bar{z} - \bar{s})].$$

For a Gaussian electron beam with rms energy spread of  $\sigma_\eta$  and centered at energy  $\eta_0$ , with the distribution function given by

$$\bar{F}(\eta) = \frac{e^{-(\eta-\eta_0)^2/2\sigma_\eta^2}}{\sqrt{2\pi}\sigma_\eta}$$

and

$$\frac{\partial \bar{F}(\eta)}{\partial \eta} = -\frac{\eta - \eta_0}{\sigma_\eta^2} \bar{F}(\eta),$$

the gain formula reduces to

$$G = h\chi_p \kappa_p n_e \int_{-L_u/2}^{L_u/2} dz \int_{-L_u/2}^{L_u/2} ds \mathcal{I}_\eta(z; s), \quad (42)$$

where

$$\begin{aligned} \mathcal{I}_\eta(z; s) &= \int d\eta \frac{\partial \bar{F}}{\partial \eta} U_\nu^*(\eta; z) U_\nu(\eta; s) \\ &= -\frac{1}{\sqrt{2\pi}\sigma_\eta^3} \int d\eta (\eta - \eta_0) e^{-(\eta-\eta_0)^2/2\sigma_\eta^2} e^{i2(\nu\eta - \Delta\nu/2)k_u(z-s)} \\ &= -2i\nu k_u(z-s) e^{i2(\nu\eta_0 - \Delta\nu/2)k_u(z-s)} \exp\{-2[k_u\nu\sigma_\eta(z-s)]^2\}. \end{aligned}$$

We got rid of bars over  $z$  and  $s$  for convenience. Finally, the gain formula reduces to

$$G = 2\nu h k_u L_u^3 \chi_p \kappa_p n_e \int_{-1/2}^{1/2} dz \int_{-1/2}^{1/2} ds (z-s) \sin[2x_0(z-s)] e^{-2[2\pi N_u \nu \sigma_\eta(z-s)]^2}, \quad (43)$$

where  $x_0 = 2\pi N_u(\nu\eta_0 - \Delta\nu/2)$ . We now replace  $\nu$  with  $p$  without breaking any assumptions of the low-gain analysis. Following Colson, we define  $j_{C,hp} = 4phk_u L_u^3 \chi_p \kappa_p n_e = h j_{C,p}$  [26]. Hence, 1D gain formulas for low-gain FEL for harmonic  $p$  upon seeding by harmonic  $h$  is given by

$$\begin{aligned} G &= \frac{j_{C,hp}}{2} \int_{-1/2}^{1/2} dz \int_{-1/2}^{1/2} ds (z-s) \sin[2x_0(z-s)] e^{-2[2\pi N_u p \sigma_\eta(z-s)]^2} \\ &= hG_1. \end{aligned} \quad (44)$$

$G_1$  represents FEL gain for harmonic  $p$  upon seeding by fundamental radiation. The above expression suggests that the FEL gain at harmonic  $p$  increases by a factor  $h$  when the seeding laser is switched from fundamental to harmonic  $h$ . This extra factor of contribution comes from the phase rate equation (7) where the harmonic  $h$  increases phase change by a factor of  $h$  compared to that of fundamental.

In addition, the FEL gain depends on the scaled detuning factor  $x_0$  and energy spread  $\sigma_\eta$ . Figure 5 shows density plot of the normalized gain  $2G/j_{C,hp}$  with respect to scaled detuning factor  $x_0$  as  $x$  axis and scaled energy spread  $y = 2\pi N_u \nu \sigma_\eta$  as  $y$  axis. Unlike spontaneous radiation which is maximized at  $x_0 \approx 0$  [see Fig. 4(a)], the maximal/minimal gain for low-gain amplification occurs at optimal detuning

$x_0 \sim \pm 1.3$  for  $y \leq 0.5$ ; the optimal detuning value shifts further away from zero for extremum gain for  $y > 0.5$  as indicated by the white lines. For  $y_0 > 2$ , the normalized gain is less than 0.05 (see also Ref. [22]). The energy spread requirements for harmonic  $p > 1$  emission are more stringent than that for fundamental emission by a factor of  $p$ . For instance,  $\sigma_\eta \leq 1/4\pi N_u$  can attain maximal gain at tuned electron energy whereas for a harmonic emission, this requirement becomes  $\sigma_\eta \leq 1/4\pi p N_u$ . This strict requirement may be relaxed a bit by harmonic seeding as discussed in the previous section. Similarly, the optimal detuned energy shift with harmonic number; the optimal energy shift  $\eta_0^p$  for a harmonic number  $p$  to maintain extremum FEL gain is given by

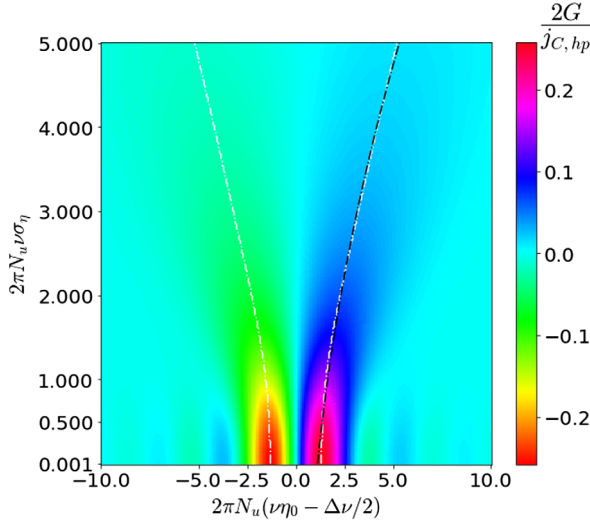


FIG. 5. Density plot of normalized gain  $2G/j_{C,hp}$  versus scaled detuning factor  $x_0 = 2\pi N_u(\nu\eta_0 - \Delta\nu/2)$  and scaled energy spread  $y = 2\pi N_u\nu\sigma_\eta$ .

$$\eta_0^p = \frac{1}{p} \left( \frac{\Delta\nu}{2} \pm \frac{f(y)}{2\pi N_u} \right), \quad (45)$$

where

$$f(y) \approx \begin{cases} 1.3 & \text{if } y \leq 0.5 \\ 0.08y^2 + 0.434y + 1.12 & \text{if } y > 0.5 \end{cases}. \quad (46)$$

Here  $f(y)$  is a fit function obtained by curve fitting to a quadratic function and is represented by the black curve in Fig. 5.

$$\mu = \frac{\sqrt[3]{p}}{2} \left[ -1 + \left( \frac{1}{3\rho\sqrt[3]{p}} - \frac{1}{3p} \right) \Delta\nu - \left( \frac{\Delta\nu}{6\rho\sqrt[3]{p}} \right)^2 + \left( \frac{\Delta\nu}{3p} \right)^2 \right] + i \frac{\sqrt[3]{p}\sqrt{3}}{2} \left[ 1 + \frac{\Delta\nu}{3p} - \left( \frac{\Delta\nu}{3p} \right)^2 - \left( \frac{\Delta\nu}{6\rho\sqrt[3]{p}} \right)^2 \right]. \quad (47)$$

Compared to Eq. (4.60) in Ref. [22], we obtain additional factors for first and second orders in  $\Delta\nu$  because Ref. [22] solves for  $\nu \equiv p = 1$  and ignores the correction factor of  $\Delta\nu$  from right-hand side of Eq. (35). The contribution to the growing radiation mode comes from the imaginary component of root in Eq. (47) which depends on harmonic number  $p$ , detuning  $\Delta\nu$ , and Pierce parameter  $\rho$ . To get a sense of this dependence, we look at the density plot of normalized growth rate  $\Im(\mu)/\sqrt[3]{p}$  as a function of  $\Delta\nu$  and  $\rho$  for certain harmonics  $p$  as shown in Fig. 6. The small offset of maximized growth rate from  $\Delta\nu = 0$  coming from the first order  $\Delta\nu/3p$  is barely noticeable in the case of fundamental ( $p = 1$ ) and 5th harmonic ( $p = 5$ ). Increasing  $p$  indicates more area of maximized growth rate for lower  $\rho \sim 10^{-5}$  and below for larger detuning width  $\Delta\nu$ , which further gets amplified by a factor of  $\sqrt[3]{p}$  for  $p > 1$ .

### C. Exponential growth

In general, we obtain all modes (growing, decaying, oscillating) for emitted radiation of Eq. (33) by setting the dispersion function to zero, i.e.,  $D(\mu) = 0$ . Since the dispersion function or its poles depend on both frequency detuning ( $\Delta\nu \neq 0$ ) and the nature of electron beam energy distribution function  $\bar{F}(\eta)$  as indicated by Eq. (34), finding exact solutions for all modes or simply growing modes can become a rigorous task; one often relies on approximate and numerical approaches (see Refs. [22,24,60,61] and references within) to study desired effects. For instance, we can obtain relevant analytical expressions for the simplest case scenario like Eq. (21) for the resonant case for a particle beam with vanishing energy spread. Now we continue to study the effects of frequency detuning from the resonant condition and nonvanishing energy spread on growth rate separately for convenience.

First, we consider the effects of  $\Delta\nu$  on growth rate in the case of vanishing energy spread as given by Eq. (35). Although Eq. (35) has roots with closed-form expressions, a simpler approach of perturbation expansion of growth rate upto the second order in  $\Delta\nu$  is enough to consider frequency detuning effects for  $\Delta\nu \ll 1$  [22]. For this, we expand  $\mu$  as

$$\mu = \mu_0 + \mu_1 \Delta\nu + \mu_2 (\Delta\nu)^2,$$

and solve for  $\mu_1$  and  $\mu_2$ , where  $\mu_0 = \sqrt[3]{p}(i\sqrt{3} - 1)/2$  is the root containing growing mode (second root) in Eq. (35). Since  $\nu = p + \Delta\nu$ , we obtain

The presence of both first order and second order terms of  $\Delta\nu$  in the imaginary component of the root means that the power of the growing mode suffers a change in gain length from resonance condition as well as the shift in central frequency with changing bandwidth. Particularly,

$$P \propto e^{4\Im(\mu)\rho k_u z} \propto e^{z/L_{g0}} \exp \left[ -\frac{1}{2} \left( \frac{\omega_\nu - \omega_{p'}}{\sigma_\omega} \right)^2 \right], \quad (48)$$

where the shifted central frequency is given by

$$\omega_{p'} = \omega_1 \left[ p + \frac{6p\rho^2}{4\rho^2 + p^{4/3}} \right] \approx \omega_1(p + 6p^{1/3}\rho),$$

and the rms frequency bandwidth is

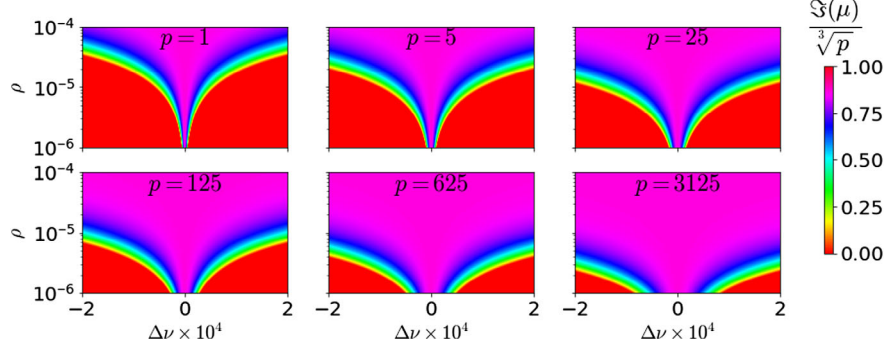


FIG. 6. Density plot of normalized growth rate  $\mathfrak{S}(\mu)/\sqrt[3]{p}$  versus frequency detuning  $\Delta\nu \times 10^4$  as x axis and Pierce parameter  $\rho$  as y axis. The y axis is in the  $\log_{10}$  scale.

$$\sigma_\omega = \omega_1 \sqrt{\frac{3\sqrt{3}\rho p^{5/3}}{k_{uz}(4\rho^2 + p^{4/3})}} \approx \omega_1 \sqrt{\frac{3\sqrt{3}\rho^{1/3}p}{k_{uz}}}. \quad (49)$$

The rms frequency bandwidth reduces to the known result  $\sigma_\nu = \sigma_\omega/\omega_1 = \sqrt{3\sqrt{3}\rho/(k_{uz})}$  of Eq. (4.61) of Ref. [22] for fundamental radiation, whereas the fundamental frequency gets shifted by  $\delta\omega_1 \approx 6\rho\omega_1$  for  $\rho \ll 1$ . Likewise, the coherence length of the growing mode becomes

$$\sigma_l = \frac{1}{2\omega_1} \sqrt{\frac{k_{uz}(4\rho^2 + p^{4/3})}{3\sqrt{3}\rho p^{5/3}}} \approx \frac{1}{2\omega_1} \sqrt{\frac{k_{uz}}{3\sqrt{3}\rho p^{1/3}}}. \quad (50)$$

The change in gain induced by frequency detuning is on the order of  $\sim\rho^3$ , which is negligible for  $\rho \ll 1$ .

The study of the exact effect of nonvanishing energy spread in the e-beam on the growth rate by solving Eq. (34) requires knowing the energy distribution function of the e-beam. While closed-form solutions are known to exist for uniform [22,28] and Lorentzian [24,62], other distribution forms such as waterbag and Gaussian necessitate adopting variational and numerical approaches [60,61,63]. Since the energy distribution functions satisfy  $\int d\eta \bar{F}(\eta) = 1$ , we can obtain simplified solution for growth rate by using perturbation expansion upto second order in  $\nu\eta/\rho$  for  $\nu \equiv p$  and  $\nu\eta/\rho \ll \Re(\mu_0)$ . Substituting

$$\mu = \mu_0 + \mu_1(p\eta/\rho) + \mu_2(p\eta/\rho)^2$$

and bringing the integral  $\int d\eta \bar{F}(\eta)$  outside in the dispersion expression of Eq. (34) gives the following solution for the second mode (containing growth mode):

$$\mu = \frac{\sqrt[3]{p}}{2} \left[ -1 + 4 \left( \frac{p^{2/3}\eta}{3\rho} \right) + \left( \frac{p^{2/3}\eta}{3\rho} \right)^2 \right] \times i \frac{\sqrt{3}\sqrt[3]{p}}{2} \left[ 1 - \left( \frac{p^{2/3}\eta}{3\rho} \right)^2 \right]. \quad (51)$$

Now we can solve for average growth rate by using  $\langle \mu \rangle = \int d\eta \mu \bar{F}(\eta)$ . For energy distributions given by

$$\bar{F}(\eta)_{\text{Un}} = \begin{cases} \frac{1}{2w_\eta} & \text{if } \eta \leq |w_\eta| \\ 0 & \text{otherwise} \end{cases}, \quad (52a)$$

$$\bar{F}(\eta)_{\text{Lor}} = \frac{w_\eta}{\pi[\eta^2 + w_\eta^2]}, \quad (52b)$$

$$\bar{F}(\eta)_{\text{Gauss}} = \frac{1}{\sqrt{2\pi}\sigma_\eta} \exp\left[-\frac{\eta^2}{2\sigma_\eta^2}\right], \quad (52c)$$

for uniform, Lorentzian and Gaussian forms respectively, we obtain,

$$\left\langle \frac{2\mathfrak{S}(\mu)}{\sqrt[3]{p}\sqrt{3}} \right\rangle = \begin{cases} 1 - \frac{1}{27} \left( \frac{p^{2/3}w_\eta}{\rho} \right)^2 & \text{for uniform,} \\ 1 - \frac{1}{9} \left( \frac{p^{2/3}w_\eta}{\rho} \right)^2 & \text{for Lorentzian,} \\ 1 - \frac{1}{9} \left( \frac{p^{2/3}\sigma_\eta}{\rho} \right)^2 & \text{for Gaussian.} \end{cases} \quad (53)$$

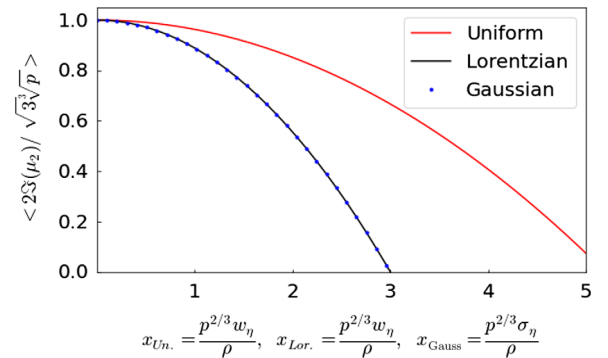


FIG. 7. Plot of normalized growth rate  $\langle \frac{2\mathfrak{S}(\mu)}{\sqrt[3]{p}\sqrt{3}} \rangle$  versus scaled energy spread factors  $x_{\text{Un}} = p^{2/3}w_\eta/\rho$  for uniform,  $x_{\text{Lor}} = p^{2/3}w_\eta/\rho$  for Lorentzian, and  $x_{\text{Gauss}} = p^{2/3}\sigma_\eta/\rho$  for Gaussian energy distribution functions.

In the above expressions,  $w_\eta$  is full(half) width at half maximum for uniform (Lorentzian) and  $\sigma_\eta$  is rms energy spread for Gaussian distributions. We find the average growth rate is attenuated faster for harmonic  $p > 1$  compared to fundamental for a given distribution. The attenuation rate is quadratic in energy spread width with a multiplicative factor of  $p^{4/3}/(3\rho)^2$ . Figure 7 shows the normalized growth rate for three different distribution functions as given by Eq. (53). The growth rate for Gaussian and Lorentzian distributions follow a similar trend and attenuates earlier compared to that for uniform distribution; however,  $x$  axis scaling is different for each distribution. For Gaussian distribution, we obtain an extrafactor of 1/9 in the correction term when compared to the textbook power gain length formulas for fundamental radiation [22].

## V. CONCLUSION

To sum up, we have derived governing equations for longitudinal FEL dynamics for harmonic lasing by harmonic seeding in the absence of transverse effects. A simple analysis allowed us to compare the FEL power of saturation for both harmonic seed and harmonic emission. We adopted collective variables to gain insight into power gain length in high-gain FELs for ideal conditions. Similarly, coupled Maxwell-Klimontovich equations allowed us to investigate spontaneous radiation and coherent amplification in low-gain and high-gain systems in the presence of both frequency detuning from resonance condition and energy spread. The model presented here allows us to generalize FEL solutions and gain expressions for harmonic emission in the presence of a harmonic seed in 1D. We hope the results obtained here could find potential applications in the design and analysis of FEL devices operating at various ranges of parameters. The extension of this work in 3D will be presented elsewhere.

## ACKNOWLEDGMENTS

This work was supported by Brookhaven Science Associates, LLC under Contract No. DE-SC0012704 with the U.S. Department of Energy and Laboratory Directed Research and Development Program at Brookhaven National Laboratory. We thank L.-H. Yu for encouraging discussions that motivated this work and T. Shaftan for reading the report. We are grateful to K.-J. Kim and R. Lindberg for introducing us to FEL physics. We acknowledge J.-W. Park for fruitful discussions on mode competition.

## APPENDIX A: SINGLE ELECTRON MOTION

For convenience, we solve for electron motion along the  $z$  axis (at  $x = 0$  and  $y = 0$ ). For the undulator period  $\lambda_u$ , the magnetic field of a planar undulator along the  $z$  axis is

$$B_y = B_0 \sin(k_u z), \quad (\text{A1})$$

where  $k_u = 2\pi/\lambda_u$  is the undulator wave number,  $B_0$  is the peak magnetic field, and the field component is along the vertical direction. For a relativistic electron with Lorentz factor  $\gamma$ , velocity  $\mathbf{v}$ , the Lorentz force equation becomes

$$\begin{aligned} \frac{d}{dt}(\gamma m \mathbf{v}) = & -e\mathbf{E} - e[\hat{x}(v_y B_z - v_z B_y) \\ & - \hat{y}(v_x B_z - v_z B_x) + \hat{z}(v_x B_y - v_y B_x)], \end{aligned} \quad (\text{A2})$$

where  $\mathbf{v} = (v_x, v_y, v_z)$  and  $v_i$  is the electron's velocity along  $i$ th direction,  $m$  is electron mass, and  $e$  is electron charge. The electric field  $\mathbf{E}$  contribution comes from the seed radiation, and by using the Lorentz force equation, we have effectively ignored the recoil effects of emitted radiation on electron motion. Since  $|\mathbf{E}| \propto \sin(kz - \omega t + \phi)$  for a radiation with frequency  $\omega$  and phase  $\phi$ , the effect of this electric field amplitude on electron velocity is proportional to  $\hbar/\gamma \ll 1$  for a relativistic electron ( $\gamma \gg 1$ ), where  $\hbar = h/2\pi$  with  $h$  being the Planck's constant. Thus, we ignore the electric field contribution in Eq. (A2) and keep the remaining contribution from the magnetic field using Eq. (A1). The magnetic field results in wiggle motion in the  $x$  direction as well as a reduction in the longitudinal velocity. Assuming electron energy loss is negligible along the undulator (generally true for low-gain FELs), it is easy to show that

$$v_x = -\frac{Kc}{\gamma} \cos(k_u z), \quad (\text{A3a})$$

$$\begin{aligned} v_z &= \sqrt{v^2 - v_x^2 - v_y^2} \\ &= c \sqrt{\left(1 - \frac{1}{\gamma^2}\right) - \left(\frac{v_x}{c}\right)^2} \\ &\approx \bar{v}_z - \frac{K^2 c}{4\gamma^2} \cos(2k_u z). \end{aligned} \quad (\text{A3b})$$

Here  $c$  is the speed of light and we introduced  $K = \frac{eB_0}{mc k_u} = 0.9343 \lambda_u [\text{cm}] B_0 [\text{T}]$  as the undulator deflection parameter. The average longitudinal electron velocity is given by  $\bar{v}_z = c[1 - \frac{1+K^2/2}{2\gamma^2}]$ . Likewise, the time  $t$  it takes an electron to arrive at location  $z$  can be obtained from  $v_z$  as follows:

$$t(z) = t(0) + \int \frac{dz}{v_z} = \bar{t}(z) + \frac{K^2}{8k_u \gamma^2 c} \sin(2k_u z), \quad (\text{A4})$$

where  $\bar{t}(z) = t(0) + \frac{z}{c}(1 + \frac{1+K^2/2}{2\gamma^2})$  represents average particle time. We refer the audience to Ref. [22] for more information.

## APPENDIX B: MAXWELL EQUATION FOR EMITTED RADIATION

The electric field amplitude of the emitted radiation due to the motion of an electron beam current in the undulator can be obtained by solving the Maxwell equation. The slowly varying envelope approximation to the paraxial wave equation results in the angular field representation given by (Eq. (3.59) of Ref. [22])

$$\begin{aligned} & \left[ \frac{\partial}{\partial z} + \frac{ik}{2} \phi^2 \right] \tilde{\mathcal{E}}_\omega(\boldsymbol{\phi}; z) \\ &= \sum_{j=1}^{N_e} \frac{e(v_{xj}/c - \phi_x)}{4\pi\epsilon_0 c \lambda^2} e^{ik[ct_j(z)-z]} \int dx e^{-ik\boldsymbol{\phi}\cdot\mathbf{x}} \delta(\mathbf{x} - \mathbf{x}_j), \end{aligned} \quad (\text{B1})$$

where  $\epsilon_0$  is the free-space permittivity and  $\lambda$  is the radiation wavelength. In one dimension, we can use the approximation  $\delta(\mathbf{x} - \mathbf{x}_j) \rightarrow \mathcal{A}_{tr}^{-1}$  with  $\mathcal{A}_{tr}$  being the transverse area. From now on, we will be using shorthand notation  $\boldsymbol{\phi}_\perp = \boldsymbol{\phi}$  for all vectors since  $z$  is an independent variable; in other words,  $\boldsymbol{\phi} = (\phi_x, \phi_y)$ . Also,  $\int dx e^{-ik\boldsymbol{\phi}\cdot\mathbf{x}} \delta(\mathbf{x} - \mathbf{x}_j) \rightarrow \mathcal{A}_{tr}^{-1} \int dx e^{-ik\boldsymbol{\phi}\cdot\mathbf{x}} = \lambda^2 \delta(\boldsymbol{\phi}) / \mathcal{A}_{tr}$ . We complete the 1D limit by defining the one-dimensional angular electric field  $\tilde{\mathcal{E}}_\omega(\boldsymbol{\phi}; z) = \tilde{E}_\omega(z) \delta(\boldsymbol{\phi}) = \tilde{E}_\nu(z) \delta(\boldsymbol{\phi})$ . Upon substituting the velocity from Eq. (A3a) and integrating over angles, Eq. (B1) becomes

$$\frac{\partial}{\partial z} \tilde{E}_\nu(z) = - \frac{eK \cos(k_u z)}{4\pi\epsilon_0 c \mathcal{A}_{tr}} \sum_{j=1}^{N_e} \frac{e^{ik[ct_j(z)-z]}}{\gamma_j}. \quad (\text{B2})$$

The slowly varying radiation field envelope requires finding slowly varying current which we can do by substituting  $t(z)$  with the average particle time from Eq. (A4). For simplicity, we will assume that only harmonic  $h$  is the dominating field providing the pondermotive potential in conjunction with the undulator field so that  $\theta \equiv \theta^h$ . This means

$$\begin{aligned} & k[ct_j(z) - z] \\ &= k \left[ c\bar{t}_j(z) + \frac{K^2}{8k_u \gamma^2} \sin(2k_u z) \right] - kz \\ &= \frac{\nu}{h} (\omega_n \bar{t}_j(z) - k_h z) + \frac{k_\nu K^2}{k_u 8\gamma^2} \sin(2k_u z) \\ &= -\frac{\nu}{h} (\theta_j^h - hk_u z) + \frac{k_\nu K^2}{k_u 8\gamma^2} \sin(2k_u z) \\ &= -\frac{\nu}{h} \theta_j^h + pk_u z + \Delta\nu k_u z + \frac{k_\nu K^2}{k_u 8\gamma^2} \sin(2k_u z), \end{aligned} \quad (\text{B3})$$

where we have substituted  $\nu = k/k_1 = \omega/\omega_1$  and  $\Delta\nu = \nu - p$  as a factor of deviation from harmonic  $p$ , where  $p$  is

not necessarily equal to  $h$ . In fact,  $p \neq h$  would allow us to explore the potential of achieving harmonic lasing via nonoverlapping harmonic seeding. Now Eq. (B2) reduces to

$$\begin{aligned} \frac{\partial}{\partial z} \tilde{E}_\nu(z) &= - \frac{eK \cos(k_u z) e^{ipk_u z} \exp \left[ i \frac{k_\nu K^2}{k_u 8\gamma^2} \sin(2k_u z) \right]}{4\pi\epsilon_0 c \mathcal{A}_{tr}} \\ &\times \sum_{j=1}^{N_e} \frac{e^{-i\nu\theta_j^h/h} e^{i\Delta\nu k_u z}}{\gamma_j}. \end{aligned} \quad (\text{B4})$$

Again applying the Jacobi-Anger identity and keeping only the terms that give rise to pondermotive phase, we can write

$$\begin{aligned} & \cos(k_u z) e^{ipk_u z} \exp \left[ i \frac{k_\nu K^2}{k_u 8\gamma^2} \sin(2k_u z) \right] \\ &= \frac{1}{2} \sum_{n=-\infty}^{\infty} J_n \left( \frac{k_\nu K^2}{k_u 8\gamma^2} \right) \left[ e^{i(1+p+2n)k_u z} + e^{-i(1-p-2n)k_u z} \right] \\ &= \frac{1}{2} \left[ J_{-(1+p)} \left( \frac{k_\nu K^2}{k_u 8\gamma^2} \right) + J_{-(p-1)} \left( \frac{k_\nu K^2}{k_u 8\gamma^2} \right) \right] \\ &= \frac{1}{2} [JJ]_p. \end{aligned}$$

In order to obtain the last expression, we used  $\nu \approx p$  for  $\Delta\nu \ll 1$ . and  $\gamma \approx \gamma_r$  for  $\eta \ll 1$ . Since we want to connect physical field to the spectral field, we define  $E_\nu(z) = \omega_1 e^{-i\Delta\nu k_u z} \tilde{E}_\nu(z)$ . Finally, Eq. (B4) takes the form

$$\begin{aligned} \left[ \frac{\partial}{\partial z} + i\Delta\nu k_u \right] E_\nu(z) &= - \frac{ek_1 K [JJ]_p}{8\pi\epsilon_0 \gamma_r \mathcal{A}_{tr}} \sum_{j=1}^{N_e} e^{-i\frac{\nu}{h}\theta_j^h} \\ &= - \frac{\kappa_p n_e}{N_{\lambda 1}} \sum_{j=1}^{N_e} e^{-i\frac{\nu}{h}\theta_j^h}. \end{aligned} \quad (\text{B5})$$

Here  $\kappa_p = \frac{eK[JJ]_p}{4e_0\gamma_r}$ ,  $N_{\lambda 1} = \lambda_1 dN_e/dz = \lambda_1 I/ec$ , and  $n_e = \frac{dN_e/dz}{\mathcal{A}_{tr}}$  is the electron volume density. We obtain the time domain wave equation from Eq. (B5) by applying Fourier transform, i.e.,  $E(\theta; z) = \int d\nu e^{i\Delta\nu\theta/h} E_\nu(z)$  as

$$\left[ \frac{\partial}{\partial z} + hk_u \frac{\partial}{\partial \theta} \right] E(\theta; z) = - \frac{2\pi\kappa_p n_e}{N_{\lambda h}} \sum_{j=1}^{N_e} e^{-ip\theta/h} \delta(\theta - \theta_j^h), \quad (\text{B6})$$

where  $N_{\lambda h} = N_{\lambda 1}/h = \lambda_h dN_e/dz$  is the number of electrons contained within harmonic wavelength  $\lambda_h$ . The derivative with respect to  $\theta$  is the slippage effect. In one undulator period, the radiation slips ahead of the emitting electron by its wavelength. For information on harmonic emission on fundamental seeding, please refer to Ref. [22].

### APPENDIX C: COMPLETE SOLUTION OF CUBIC EQUATION

The cubic equation (20) has been solved for fundamental seeding case [22,24]. Here we solve for the complete solution for harmonic seed and harmonic emission by seeking solution of the form  $a(\hat{z}) \propto e^{r\hat{z}}$ ; the three roots for this solution form are  $\sqrt[3]{p}[e^{-i\pi/2}, e^{i\pi/6}, e^{i5\pi/6}]$ . The first root gives rise to the oscillatory solution, whereas the second and third roots give rise to growing and damping solutions, respectively, in addition to the oscillating components. The complete solution for the field amplitude is given by

$$a(\hat{z}) = \sum_{n=1}^3 c_n e^{r_n \hat{z}}, \quad (\text{C1})$$

where the constants  $c_1$ ,  $c_2$ , and  $c_3$  are determined by the initial conditions. Writing the initial values as  $a(0) = a_0$ ,  $b_h(0) = b_0$ , and  $\mathcal{P}_c(0) = \mathcal{P}_0$ , the initial values give

$$\begin{aligned} c_1 + c_2 + c_3 &= a_0, \\ r_1 c_1 + r_2 c_2 + r_3 c_3 &= -b_0, \\ r_1^2 c_1 + r_2^2 c_2 + r_3^2 c_3 &= ip\mathcal{P}_0. \end{aligned} \quad (\text{C2})$$

Solving for the coefficients yield

$$\begin{aligned} c_1 &= \frac{r_2 r_3 a_0 + [(r_2 + r_3)b_0 + ip\mathcal{P}_0]}{(r_1 - r_2)(r_1 - r_3)}, \\ c_2 &= \frac{r_1 r_3 a_0 + [(r_1 + r_3)b_0 + ip\mathcal{P}_0]}{(r_2 - r_1)(r_2 - r_3)}, \\ c_3 &= \frac{r_1 r_2 a_0 + [(r_1 + r_2)b_0 + ip\mathcal{P}_0]}{(r_3 - r_2)(r_3 - r_1)}. \end{aligned} \quad (\text{C3})$$

Using the fact that  $\sum_{n=1}^3 r_n = 0$  and  $\sum_{n=1}^3 \frac{1}{r_n} = 0$  along with basic properties such as  $(r_l - r_m)(r_l - r_n) = 3r_m r_n$  for  $l \neq m \neq n$ , the complete solution of the cubic equation takes the following form:

$$a(\hat{z}) = \frac{1}{3} \sum_{n=1}^3 \left[ a_0 - \frac{b_0}{r_n} + r_n \mathcal{P}_0 \right] e^{r_n \hat{z}}. \quad (\text{C4})$$

- [1] J. M. J. Madey, *J. Appl. Phys.* **42**, 1906 (1971).  
 [2] J. Rossbach, J. R. Schneider, and W. Wurth, *Phys. Rep.* **808**, 1 (2019), 10 years of pioneering X-ray science at the Free-Electron Laser FLASH at DESY.  
 [3] C. Bostedt, S. Boutet, D. M. Fritz, Z. Huang, H. J. Lee, H. T. Lemke, A. Robert, W. F. Schlotter, J. J. Turner, and G. J. Williams, *Rev. Mod. Phys.* **88**, 015007 (2016).

- [4] M. Yabashi, H. Tanaka, K. Tono, and T. Ishikawa, *Appl. Sci.* **7**, 604 (2017).  
 [5] E. Allaria *et al.*, *J. Synchrotron Radiat.* **22**, 485 (2015).  
 [6] I. Eom, S. H. Chun, J. H. Lee, D. Nam, R. Ma, J. Park, S. Park, S. H. Park, H. Yang, I. Nam, M. H. Cho, C. H. Shim, G. Kim, C.-K. Min, H. Heo, H.-S. Kang, and C. Kim, *Appl. Sci.* **12**, 1010 (2022).  
 [7] C. J. Milne *et al.*, *Appl. Sci.* **7**, 720 (2017).  
 [8] Z. Zhao, D. Wang, Q. Gu, L. Yin, G. Fang, M. Gu, Y. Leng, Q. Zhou, B. Liu, C. Tang, W. Huang, Z. Liu, and H. Jiang, *Synchrotron Radiat. News* **30**, 29 (2017).  
 [9] Z. Zhu, Z. T. Zhao, D. Wang, Z. H. Yang, and L. Yin, in *Proceedings of FEL'17 (JACoW, Geneva, Switzerland, 2017)*, pp. 182–184, <https://refs.jacow.org/reference/show/91354>.  
 [10] T. Kolodziej, Y. Shvyd'ko, D. Shu, S. Kearney, S. Stoupin, W. Liu, T. Gog, D. A. Walko, J. Wang, A. Said, T. Roberts, K. Goetze, M. Baldini, W. Yang, T. Fister, V. Blank, S. Terentyev, and K.-J. Kim, *J. Synchrotron Radiat.* **25**, 1022 (2018).  
 [11] T. Kolodziej, S. Stoupin, W. Grizolli, J. Krzywinski, X. Shi, K.-J. Kim, J. Qian, L. Assoufid, and Y. Shvyd'ko, *J. Synchrotron Radiat.* **25**, 354 (2018).  
 [12] Z. Huang and R. D. Ruth, *Phys. Rev. Lett.* **96**, 144801 (2006).  
 [13] K.-J. Kim, Y. Shvyd'ko, and S. Reiche, *Phys. Rev. Lett.* **100**, 244802 (2008).  
 [14] R. R. Lindberg, K.-J. Kim, Y. Shvyd'ko, and W. M. Fawley, *Phys. Rev. ST Accel. Beams* **14**, 010701 (2011).  
 [15] R. R. Lindberg, K. J. Kim, Y. Cai, Y. Ding, and Z. Huang, in *Proceedings of the 35th International Free-Electron Laser Conference, FEL2013, New York, NY (JACoW Publishing, Geneva, Switzerland, 2013)*, Vol. 2, pp. 740–748, <https://jacow.org/FEL2013/papers/THOBN002.pdf>.  
 [16] I. Agapov, Y. Chae, and W. Hillert, in *Proceedings of the 9th International Particle Accelerator Conference, IPAC2018, Vancouver, BC, Canada (JACoW, Geneva, Switzerland, 2018)*, p. 1420.  
 [17] G. Marcus, F. J. Decker, G. L. Gassner, A. Halavanau, J. Hastings, Z. Huang, Y. Liu, J. MacArthur, R. Margraf, T. Raubenheimer, A. Sakdinawat, T. Tan, D. Zhu, J. W. Anton, L. Assoufid, K. Goetze, W. Jansma, S. Kearney, K. J. Kim, R. Lindberg, A. Miceli, X. Shi, D. Shu, Y. Shvyd'ko, J. P. Sullivan, M. White, and B. Lantz, in *Proceedings of the 39th International Free-Electron Laser Conference, FEL 2019, Hamburg, Germany (JACoW Publishing, Geneva, Switzerland, 2019)*, pp. 282–287, <https://jacow.org/fel2019/papers/TUD04.pdf>.  
 [18] L. H. Yu, in *Proceedings of IPAC'21 (JACoW Publishing, Geneva, Switzerland, 2021)* pp. 178–181, <https://inspirehep.net/literature/1926775>.  
 [19] P. Rauer, A proof-of-principle cavity-based x-ray free-electron-laser demonstrator at the European XFEL, Ph.D. thesis, Universitt of Hamburg, Hamburg, 2022, <https://bib-pubdb1.desy.de/record/478856>.  
 [20] Y. Li, R. Lindberg, and K.-J. Kim, *Phys. Rev. Accel. Beams* **26**, 030702 (2023).  
 [21] C. A. Brau, *Free Electron Lasers* (Academic Press, New York, 1990).

- [22] K.-J. Kim, Z. Huang, and R. Lindberg, *Synchrotron Radiation and Free-Electron Lasers: Principles of Coherent X-Ray Generation* (Cambridge University Press, Cambridge, England, 2017).
- [23] R. Margraf *et al.*, in *Proceedings of FEL2022, Trieste, Italy* (2022), paper WEP13, unpublished.
- [24] C. Pellegrini, A. Marinelli, and S. Reiche, *Rev. Mod. Phys.* **88**, 015006 (2016).
- [25] W. B. Colson, *Phys. Lett.* **64A**, 190 (1977).
- [26] W. Colson, *IEEE J. Quantum Electron.* **17**, 1417 (1981).
- [27] R. Bonifacio, C. Pellegrini, and L. Narducci, *Opt. Commun.* **50**, 373 (1984).
- [28] K.-J. Kim, *Nucl. Instrum. Methods Phys. Res., Sect. A* **250**, 396 (1986).
- [29] K.-J. Kim, *Phys. Rev. Lett.* **57**, 1871 (1986).
- [30] K.-J. Kim, *Nucl. Instrum. Methods Phys. Res., Sect. A* **318**, 489 (1992).
- [31] R. Bonifacio, L. De Salvo, and P. Pierini, *Nucl. Instrum. Methods Phys. Res., Sect. A* **293**, 627 (1990).
- [32] Z. Huang and K.-J. Kim, *Phys. Rev. E* **62**, 7295 (2000).
- [33] H. Freund, S. Biedron, and S. Milton, *IEEE J. Quantum Electron.* **36**, 275 (2000).
- [34] B. W. J. McNeil, G. R. M. Robb, M. W. Poole, and N. R. Thompson, *Phys. Rev. Lett.* **96**, 084801 (2006).
- [35] E. A. Schneidmiller and M. V. Yurkov, *Phys. Rev. ST Accel. Beams* **15**, 080702 (2012).
- [36] L. H. Yu, *Phys. Rev. A* **44**, 5178 (1991).
- [37] L. H. Yu and J. Wu, *Nucl. Instrum. Methods Phys. Res., Sect. A* **483**, 493 (2002).
- [38] G. Penn, M. Reinsch, and J. S. Wurtele, *Phys. Rev. ST Accel. Beams* **9**, 060702 (2006).
- [39] G. Stupakov, *Phys. Rev. Lett.* **102**, 074801 (2009).
- [40] D. Xiang and G. Stupakov, *Phys. Rev. ST Accel. Beams* **12**, 030702 (2009).
- [41] H. Deng and C. Feng, *Phys. Rev. Lett.* **111**, 084801 (2013).
- [42] C. Feng, H. Deng, D. Wang, and Z. Zhao, *New J. Phys.* **16**, 043021 (2014).
- [43] T. Tran and J. Wurtele, *Comput. Phys. Commun.* **54**, 263 (1989).
- [44] L. H. Yu, *Phys. Rev. E* **58**, 4991 (1998).
- [45] W. M. Fawley, A User Manual for GINGER and its post-processor XPLOTGIN, Lawrence Berkeley National Laboratory Technical Report No. LBNL-49625 Rev. 1, 2004.
- [46] S. Reiche, *Nucl. Instrum. Methods Phys. Res., Sect. A* **429**, 243 (1999).
- [47] E. Saldin, E. Schneidmiller, and M. Yurkov, *Nucl. Instrum. Methods Phys. Res., Sect. A* **429**, 233 (1999).
- [48] L. T. Campbell and B. W. J. McNeil, *Phys. Plasmas* **19**, 093119 (2012).
- [49] H. P. Freund, P. J. M. van der Slot, D. L. A. G. Grimminck, I. D. Setija, and P. Falgari, *New J. Phys.* **19**, 023020 (2017).
- [50] L. H. Yu, Medium energy hard x-ray FEL gain, National Synchrotron Light Source II, Brookhaven National Laboratory Technical Report No. NSLSII-ASD-TN-334, 2020.
- [51] Z. Huang and K.-J. Kim, *Phys. Rev. ST Accel. Beams* **10**, 034801 (2007).
- [52] S. Ichimaru, *Basic Principles of Plasma Physics* (CRC Press, Boca Raton, FL, 1973).
- [53] P. Tolias, The Klimontovich description of complex plasma systems: Low frequency electrostatic modes, spectral densities of fluctuations and collision integrals, Doctoral thesis, KTH Royal Institute of Technology, Stockholm, 2012, <https://www.diva-portal.org/smash/record.jsf?pid=diva2:510526>.
- [54] J.-M. Wang and L.-H. Yu, *Nucl. Instrum. Methods Phys. Res., Sect. A* **250**, 484 (1986).
- [55] X. Wang *et al.*, *Nat. Commun.* **4**, 1988 (2013).
- [56] A. J. Gonsalves *et al.*, *Phys. Rev. Lett.* **122**, 084801 (2019).
- [57] C. Aniculaesei, V. B. Pathak, K. H. Oh, P. K. Singh, B. R. Lee, C. I. Hojbota, T. G. Pak, E. Brunetti, B. J. Yoo, J. H. Sung, S. K. Lee, H. T. Kim, and C. H. Nam, *Phys. Rev. Appl.* **12**, 044041 (2019).
- [58] C. Aniculaesei *et al.*, High-charge 10 GeV electron acceleration in a 10 cm nanoparticle-assisted hybrid wakefield accelerator, arXiv:2207.11492.
- [59] C. Berger, S. Barber, F. Isono, K. Jensen, J. Natal, A. Gonsalves, and J. van Tilborg, *Phys. Rev. Accel. Beams* **26**, 032801 (2023).
- [60] L. H. Yu, S. Krinsky, and R. L. Gluckstern, *Phys. Rev. Lett.* **64**, 3011 (1990).
- [61] M. Xie, *Nucl. Instrum. Methods Phys. Res., Sect. A* **445**, 59 (2000).
- [62] G. T. Moore, *Nucl. Instrum. Methods Phys. Res., Sect. A* **239**, 19 (1985).
- [63] S. Krinsky and L. H. Yu, *Phys. Rev. A* **35**, 3406 (1987).